Japanese Journal of Applied Physics
Vol. 44, No. 2, 2005, pp. L88–L91



# Atomic Force Microscope Current-Imaging Study for Current Density through Nanocrystalline Silicon Dots Embedded in $SiO_2$

Mohamed Ali SALEM*, Hiroshi MIZUTA[1], Shunri ODA†, Ying FU[2] and Magnus WILLANDER[2]

*Quantum Nanoelectronics Research Center, Tokyo Institute of Technology, 2-12-1 O-okayama, Meguro-ku, Tokyo 152-8552, Japan*
[1]*Department of Physical Electronics, Tokyo Institute of Technology, 2-12-1 O-okayama, Meguro-ku, Tokyo 152-8552, Japan*
[2]*Microelectronics Center at Chalmers and Department of Physics, University of Goteborg and Chalmers University of Technology, Fysikgrdand 3, S-412 96 Goteborg, Sweden*

(Received August 12, 2004; accepted November 2, 2004; published December 17, 2004)

Simultaneous surface and current imaging through nanocrystalline silicon (nc-Si) dots embedded in $SiO_2$ was achieved using a contact mode atomic force microscope (AFM) under a tip-to-sample bias voltages of about 5 V. The obtained images were then analyzed using a one-dimensional model of current density, which took account of the spherical shape of the nc-Si dots, the substrate orientation and the sample bias. A comparison between the experimental and theoretical results showed a fair agreement when the current pass through the dot center, although a large difference was found at a higher voltage. In addition, our model predicted tunneling current oscillations due to a change in tip position relative to the dot center.
[DOI: 10.1143/JJAP.44.L88]

KEYWORDS: silicon quantum dot, atomic force microscope, current imaging, current density

Nanocrystalline silicon (nc-Si) has attracted considerable interest in recent years due to its potential applications in advanced devices such as memory elements,[1,2] electron emitter devices[3] and single-electron transistors.[4] It also provides a unique system for investigating the physics of quantum confinement effects and the associated electron transport due to its small dimensions and controlled geometry of the dots.

There are many studies on electron transport through nanocluster structures formed with one-dimensional dot arrays.[5,6] Nanostructures have been fabricated by a combination of thin-film and lithographic technologies. This facilitates the creation of devices with carefully tailored geometries and electron densities, for example, quantum dots. Although lithographic limitations restrict the minimum size of such dots, the transport measurements of these dots have provided a wealth of information about the effect of coulomb interactions and spatial quantization upon electron transport.

Electrical measurements for such structures are carried out using two approaches. The first approach relies on a system fabricated particularly for providing stable nanoscale devices, for example, single-electron transistors based on nc-Si,[7] Coulomb blockade and level quantization in Al grains that formed over a nanometer sized aperture[8] and the utilization of ion beams for depositing several AuPd nanocrystals between Au leads.[9] The second approach is the use of scanning probe microscopy that enables the local probing of sample properties giving an advantage over traditional macroscopic current and capacitance-voltage measurements.[10] A scanning tunneling microscope (STM) has been widely used for characterizing the electrical properties of nanostructures.[11–14] Important results such as the observation of single-electron charging in Si nanocrystals have been reported.

A conducting-tip atomic force microscope (C-AFM) is preferred due to its advantages over STM: the C-AFM does not require ultrahigh vacuum and any special sample treatments. Moreover, it is particularly suitable for the analysis of insulating surfaces, allowing the study of the morphological and electrical characteristics of ultrathin $SiO_2$,[15–18] and nanoparticles embedded in $SiO_2$.[19,20] Therefore, we adopt this technique to investigate electron transport through individual nc-Si dots by analyzing the current density through nc-Si dots embedded in a $SiO_2$ layer. The experimental results are analyzed using a theoretical model, which we proposed previously for evaluating the amount of charge injected into a localized area of an nc-Si dot ensemble by analyzing the height change (or apparent height) of the dot ensemble upon charge injection.[21]

Nanocrystalline Si dots were deposited on a [100] oriented $n^+$-Si (0.01 Ω cm) substrate. The nc-Si dots with diameters of $8 \pm 1$ nm were deposited on this substrate at room temperature by plasma chemical vapor deposition CVD, whose details are described elsewhere.[22] The CVD system includes a plasma cell, which is separated from a UHV chamber by a stainless steel plate with a 6 mm-diameter orifice. Ar and $SiH_4$ gases, whose flow rates were 20 and 1 sccm, respectively, were excited by a 144 MHz plasma with a power of 5 W. For the fine control of the growth of the dots, the $SiH_4$ gas was introduced as pulses of 0.1 second on and 1 second off. The nc-Si dots were formed in the gas phase by the coalescence of $SiH_4$-derived radicals and extracted out of the plasma cell through the orifice to the Si substrate. Si dots were randomly deposited on a $1 \times 1\,cm^2$ substrate. The dot density as calculated from the images is about $3.5 \times 10^9\,cm^{-2}$. Such a density is sufficiently low to examine a single nc-Si dot.

Figure 1 shows a schematic diagram of the nc-Si dots and the AFM tip under investigation. The $SiO_2$ layer was deposited by chemical vapor deposition. The flow rates of the $O_2$ and TEOS gases were 300 and 2 sccm, respectively. The RF plasma power was 250 W. The $SiO_2$ thickness was 7 nm as measured by ellipsometry. A sharp silicon tip of 5 nm radius of curvature, coated with, rhodium metal with a thickness of 30 nm, was used in the C-AFM measurements. The scan speed was 5 Hz. A surface image (Fig. 2) of $208 \times 208\,nm^2$ was scanned simultaneously with current measurements. the advantage of the simultaneous measurement of

*E-mail address: masalem@diana.pe.titech.ac.jp
†E-mail address: soda@pe.titech.ac.jp

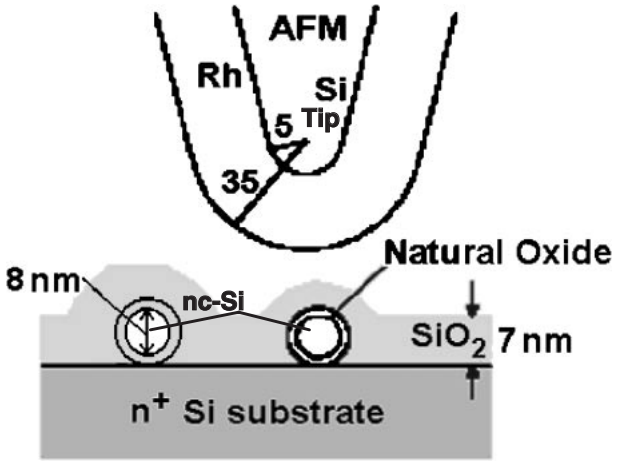


Fig. 1. Schematic drawing of the tip-sample cross section. The conductive AFM tip is 5 nm-radius silicon core coated with 35 nm thick rhodium metal. The silicon dots with an average diameter of 8 nm are embedded in the CVD $SiO_2$ layer.

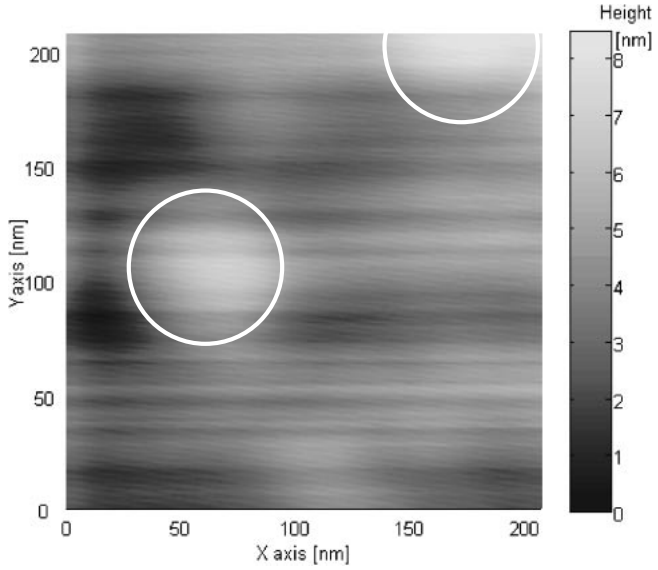


Fig. 2. Contact mode AFM surface topography image. The gray scale indicates height in nm. White circles indicate the positions of two silicon dots.

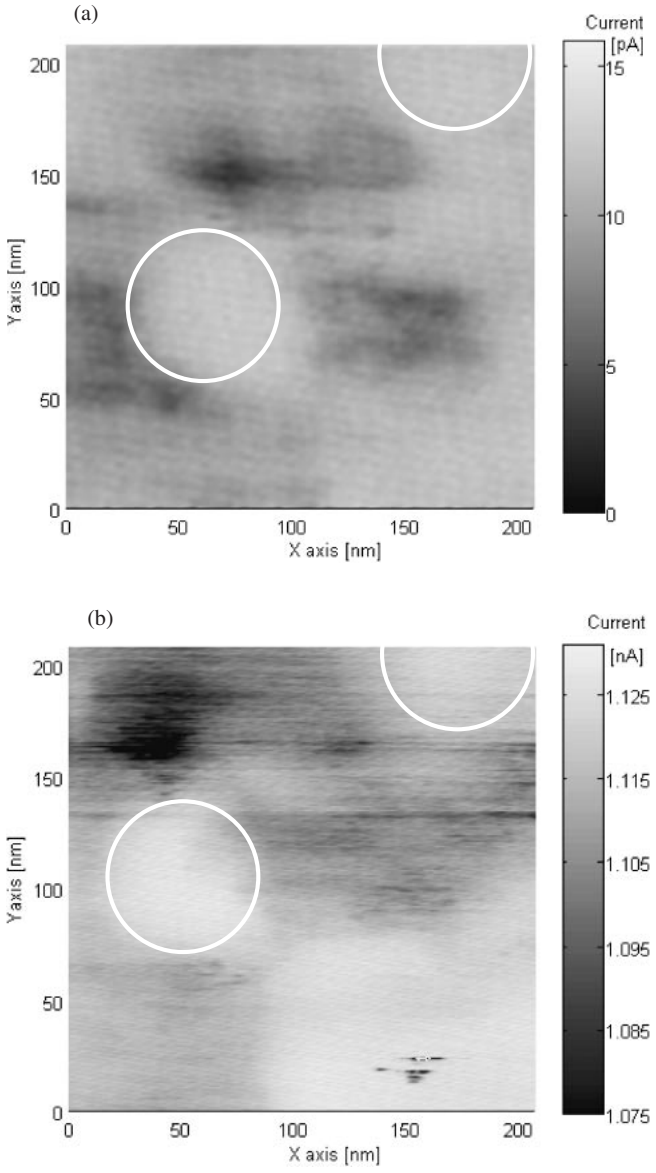


Fig. 3. AFM current images at tip-sample biases of (a) 5 V and (b) 6 V. The gray scale indicates current. The lower right region of the current image at 6 V clearly indicates the precursor of $SiO_2$ breakdown.

topography and current is that it eliminates the position discrepancy between the two types of image. The tip-sample voltage was set to be 5 V (Fig. 3(a)) and 6 V (Fig. 3(b)). From the surface topography image, we can observe two high (bright) areas: one near the image center and the other on the top right corner, indicating the positions of two nc-Si dots covered by the $SiO_2$ layer. The separation between them is about 100 nm, which is greater than the tip diameter, recalling the fact that the diameter of the tip-sample contact area is significantly smaller than the tip diameter. We then carried out a current measurement over a single silicon dot. It should be noted that the AFM images are convolutions of sample and tip geometries,[23] which suggests an additional lateral dimension increment to the actual dimension. Therefore, a spherical nanoparticle appears as a hemisphere with a diameter larger than its height.

Current images at 5 V and 6 V show that the current that passes through a dot is higher than that through an area without a dot (intense current is brighter). Furthermore, the current that passes at 6 V is larger than the current passes at 5 V. A further decrease in tip-sample bias shows less contrast, and consequently, information deduction becomes more difficult. While increasing the tip-sample bias results in the breakdown of the silicon oxide layer and reach the maximum current limit, it is important to note the precursor of such breakdown of the $SiO_2$ layer in the lower right region of the images where silicon dot is absent. This precursor is more obvious in the current image scanned at 6 V.

We consider a single nc-Si dot located at $x^2 + y^2 + (z-4)^2 = r_o^2$, where $r_o = 4$ nm is the Si dot radius. The one-dimensional transmission model is schematically shown in Fig. 4, Where

$$r^2(x,y) = \begin{cases} r_o^2 - (x^2+y^2) & \text{if } x^2+y^2 \le r_o^2 \\ 0 & \text{otherwise} \end{cases} \quad (1)$$

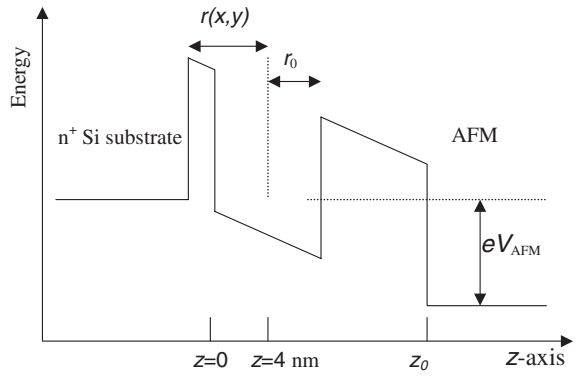


Fig. 4. Energy band profile of the one-dimensional transmission model, the origin of the $z$-axis is assumed to be at the lower edge of the silicon dot.

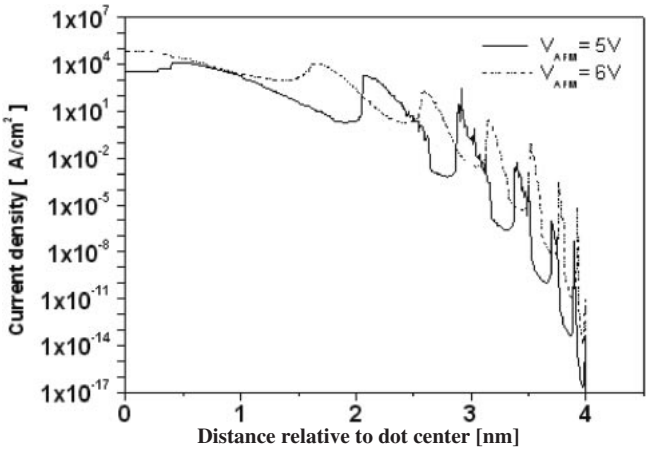


Fig. 5. Spatial distribution profile of current density along the $x$-axis at $T = 300\,\mathrm{K}$ (dashed line for $V_{\mathrm{AFM}} = 6\,\mathrm{V}$, while solid line for $V_{\mathrm{AFM}} = 5\,\mathrm{V}$).

$z_0$ is the spatial separation between the AFM probe and the $n^+$ Si substrate.

The conduction band of Si consists of six ellipsoids described by the longitudinal effective mass $m_{\mathrm{l}} = 0.98$ and the transverse effective mass $m_{\mathrm{t}} = 0.19$ expressed in units of the free electron mass $m_0$. The single-electron Hamiltonian is expressed as

$$H = -\frac{\hbar^2}{2m_x^*}\frac{\partial^2}{\partial x^2} - \frac{\hbar^2}{2m_y^*}\frac{\partial^2}{\partial y^2} - \frac{\hbar^2}{2m_z^*}\frac{\partial^2}{\partial z^2} + V(x,y,z) \quad (2)$$

in the effective mass approximation. For the two ellipsoids along the [100]-axis, $m_x^* = m_{\mathrm{l}}$, $m_y^* = m_z^* = m_{\mathrm{t}}$. V ($r$) consists of the following two parts:

(1) By setting the conduction band edge of silicon at zero in the spatial regions of the dots, the conduction band offset of the surrounding $SiO_2$ assumes $V_{\mathrm{b}} = 3.5\,\mathrm{eV}$, and the corresponding energy dispersion relation is described by the effective mass $m_{\mathrm{ox}} = 0.5$.

(2) The potential energy induced by the AFM bias is modeled as

$$\begin{cases} 0 & z < 0 \\ -eV_{\mathrm{AFM}}\dfrac{z}{z_o} & 0 \le z < z_o \\ -eV_{\mathrm{AFM}} & \text{otherwise} \end{cases} \quad (3)$$

Where $V_{\mathrm{AFM}}$ is the AFM bias. It is worth to mention that, the three-dimensional geometrical relation between the dot and the tip was not considered in this work for simplicity.

Figure 5 shows the current density on the $xy$ plane. Due to the spherical symmetry of the nc-Si dot, we set $y = 0$. With $V_{\mathrm{AFM}} = 5\,\mathrm{V}$, the current density at $x = 0$ is $0.35 \times 10^4\,\mathrm{A/cm^2}$, whereas at $V_{\mathrm{AFM}} = 6\,\mathrm{V}$, it increases to $6.44 \times 10^4\,\mathrm{A/cm^2}$. If we assume the contact area between the AFM probe and the sample as $10^{-14}\,\mathrm{cm^2}$, the corresponding peak currents are 0.035 and 0.644 nA, respectively. Taking a finite size of the contact area between the AFM probe and the sample into consideration, these values agree well with the measured peak current data. This fact proves that the electrons indeed tunnel from the substrate to the AFM probe via the nc-Si dot. The transmission is more effective along the axis perpendicular to the substrate because of a relatively thin energy barrier. The in-plane scale of the AFM images (Figs. 2 and 3) is much larger than the geometrical scale in Fig. 5 because of the large curvature of the probe compared to the in-plane geometric resolution. In addition, the model also shows resonance peaks in Fig. 5 due to the quasi-local states formed in the nc-Si dot in Fig. 4. Resonance peaks are however not observable in the present AFM measurements due to the large curvature of the probe.

We have prepared the sparse nc-Si dots on the n-type Si substrate and investigated the tunneling current through them by AFM measurements. By comparing the experimental results with the theoretical ones obtained using an effective one-dimensional electron transmission model, we have shown that the transmission current is maximal when the AFM probe sits on the top of an nc-Si dot, while it is minimal when the AFM probe is positioned in the space between the nc-Si dots. Despite the fact that this calculation method is simple and consequently describes a limited case, its results were found to be in consistency with the experimental results. Therefore these results confirm the validity of the present C-AFM-based characterization method as well as one-dimensional modeling.

The authors would like to express their gratitude to Dr. K. Usami for his help in the sample preparation and also to Dr. Y. Tsuchiya for the thorough discussion. This work was financially supported by CREST, JST.

1) S. Banerjee, S. Huang, T. Yamanaka and S. Oda: J. Vac. Sci. & Technol. B **20** (2002) 1135.
2) B. J. Hinds, T. Yamanaka and S. Oda: J. Appl. Phys. **90** (2001) 6402.
3) K. Nishiguchi, X. Zhao and S. Oda: J. Appl. Phys. **92** (2002) 2748.
4) Y. Fu, M. Willander, A. Dutta and S. Oda: Superlattices & Microstruct. **28** (2000) 189.
5) T. Sato and H. Ahmed: Appl. Phys. Lett. **70** (1997) 2759.
6) D. L. Klein, P. L. McEuen, J. E. B. Katari, R. Roth and A. P. Alivisato: Appl. Phys. Lett. **68** (1996) 2574.
7) A. Dutta, S. Oda, Y. Fu and M. Willander: Jpn. J. Appl. Phys. **39** (2000) 4647.
8) D. C. Ralph, C. T. Black and M. Tinkham: Phys. Rev. Lett. **74** (1995) 3241.
9) W. Chen, H. Ahmed and K. Nakazoto: Appl. Phys. Lett. **66** (1995) 3383.
10) Y. Shi, K. Saito, H. Ishikuro and T. Hiramoto: J. Appl. Phys. **84** (1998) 2358.
11) M. F. Crommie, C. P. Lutz and D. N. Egler: Phys. Rev. B **48** (1993) 2851.

12) M. Fukuda, N. Nakagawa, S. Miyazaki and M. Hirose: Appl. Phys. Lett. **70** (1997) 2291.
13) S. Ogawa, F. R. F. Fan and A. J. Bard: J. Phys. Chem. **99** (1995) 11182.
14) T. Baron, P. Gentile, N. Magnea and P. Mur: Appl. Phys. Lett. **79** (2001) 1175.
15) S. Kremmer, C. Teichert, E. Pischler, H. Gold, F. Kuchar and M. Schatzmayer: Surf. Interface Anal. **33** (2002) 168.
16) S. J. O'Shrea, R. M. Atta, M. P. Murrell and M. E. Welland: J. Vac. Sci. & Technol. B **13** (1995) 1945.
17) M. Porti, A. Nafria, X. Aymerich, A. Olbrich and B. Ebersberger: J. Appl. Phys. **91** (2002) 2071.
18) M. Otobe, H. Yajima and S. Oda: Appl. Phys. Lett. **72** (1998) 1089.
19) M. Fujii, O. Mamezaki, S. Hayashi and K. Yamamoto: J. Appl. Phys. **83** (1998) 1507.
20) D. M. Schaadt, E.T. Yu, S. Sankar and A. E. Berkowitz: Appl. Phys. Lett. **74** (1999) 472.
21) S. Banerjee, M. A. Salem and S. Oda: Appl. Phys. Lett. **83** (2003) 3788.
22) T. Ifuku, M. Otobe, A. Itoh and S. Oda: Jpn. J. Appl. Phys. **36** (1997) 4031.
23) T. Junno, K. Deppert, L. Montelius and L. Samuelson: Appl. Phys. Lett. **66** (1995) 3627.